

1 **Brief Communication: Newly developing rift in Larsen C Ice**
2 **Shelf presents significant risk to stability**

3

4 Daniela Jansen¹, Adrian J. Luckman², Alison Cook², Suzanne Bevan², Bernd Kulessa², Bryn
5 Hubbard³, Paul R. Holland⁴

6

7 [1] {Alfred-Wegener-Institut Helmholtz-Zentrum für Polar- und Meeresforschung,
8 Bremerhaven, Germany}

9 [2] { Department of Geography, College of Science, Swansea University, UK }

10 [3] {Centre for Glaciology, Institute for Geography and Earth Sciences, Aberystwyth
11 University, UK}

12 [4] {British Antarctic Survey, High Cross, Cambridge, UK }

13 Correspondence to: Daniela Jansen (Daniela.jansen@awi.de)

14

15 **Abstract**

16 An established rift in the Larsen C Ice Shelf, formerly constrained by a suture zone containing
17 marine ice, grew rapidly during 2014 and is likely in the near future to generate the largest
18 calving event since the 1980s and result in a new minimum area for the ice shelf. Here we
19 investigate the recent development of the rift, quantify the projected calving event and, using
20 a numerical model, assess its likely impact on ice shelf stability. We find that the ice front is
21 at risk of becoming unstable when the anticipated calving event occurs.

22

23 **1 Introduction**

24 The Larsen C Ice Shelf is the most northerly of the remaining major Antarctic Peninsula
25 ice shelves and is vulnerable to changes in both to ocean and atmospheric forcing (Holland et
26 al., 2015). It is the largest ice shelf in the region and its loss would lead to a significant
27 drawdown of ice from the Antarctic Peninsula Ice Sheet (APIS). There have been
28 observations of widespread thinning (Shepherd et al., 2003; Pritchard et al., 2012; Holland et
29 al., 2015), melt ponding in the northern inlets (Holland et al., 2011; Luckman et al., 2014),
30 and a speed-up in ice flow (Khazendar et al., 2011), all processes which have been linked to
31 former ice shelf collapses (e.g. van den Broeke, 2005). Previous studies have highlighted the
32 vulnerability of Larsen C Ice Shelf to specific potential changes in its geometry including a
33 retreat from the Bawden Ice Rise (Kulesa et al., 2014; McGrath et al., 2014; Holland et al.,
34 2015) and Gipps Ice Rise (Borstad et al., 2013). Rift tips in the latter area have been observed
35 to align as they terminate at a confluence of flow units within the shelf. Several studies have
36 provided evidence for marine ice in these *suture zones* (Holland et al., 2009; Jansen et al.,
37 2013; Kulesa et al., 2014; McGrath et al., 2014). The relatively warm, and thus soft, marine
38 ice has been found to act as a weak coupling between flow units with different flow
39 velocities. It has been concluded that this ice inhibits the propagation of rifts because it can
40 accommodate strain in the ice without fracturing further (Holland et al., 2009; Jansen et al.,
41 2013; Kulesa et al., 2014).

42 In a change from the usual pattern, a northwards-propagating rift from Gipps Ice Rise has
43 recently penetrated through the suture zone and is now more than halfway towards calving off
44 a large section of the ice shelf (Figs. 1 and 2). The rate of propagation of this rift accelerated
45 during 2014. When the next major calving event occurs, the Larsen C Ice Shelf is likely to
46 lose around 10% of its area to reach a new minimum both in terms of direct observations, and
47 possibly since the last interglacial period (Hodgson et al., 2006).

48 Here, using satellite imagery and numerical modelling, we document the development of
49 the rift over recent years, predict the area of ice that will be lost, and test the likely impact of
50 this future calving event on ice shelf stability.

51 **2 Methods**

52 **2.1 Satellite Observations**

53 We use data from NASA MODIS at a pixel size of 250 m (red band) from the near-real-
54 time archive (<http://lance-modis.eosdis.nasa.gov/cgi-bin/imagery/realtime.cgi>) to monitor the
55 general propagation of the rift and to explore its likely future path (Fig. 1). These data,
56 however, did not provide sufficiently high spatial resolution to measure the rift tip position
57 with satisfactory precision. Using Landsat data at high spatial resolution (15m, panchromatic)
58 from the NASA archive (<http://earthexplorer.usgs.gov/>), we measure in detail the rift's recent
59 propagation (Fig. 2). Growth of the rift is assessed by digitizing the position of the rift tip in
60 all Landsat images unobscured by cloud between Nov. 2010 and Jan. 2015 working within the
61 Polar Stereographic map projection in which the data were provided. The start of this
62 sequence is chosen to show normal behaviour of the rift over three years before its more rapid
63 propagation in 2014. Between January 2015 and the final paper submission, no additional
64 images showed notable further propagation. Rift length is presented relative to the position in
65 Nov. 2010 prior to the breach of the Joerg Peninsula suture zone. Rift width is measured at
66 the Nov. 2010 rift tip position. These satellite data are subject to variable cloud conditions and
67 solar illumination, the impact of which we minimize by optimizing brightness and contrast in
68 each image separately. Nevertheless, measurements of rift tip position and width are
69 potentially subject to error of up to a few tens of meters. A table listing all Landsat images
70 used for this study as well as the measured rift lengths and widths can be found in the
71 supplementary material.

72 To investigate a range of possible outcomes from the proposed calving event, we present
73 two scenarios for the rift trajectory based on its current orientation and direction of
74 propagation, and on visual inspection of MODIS data (Fig. 1). Surface features in these data
75 indicate the scale and orientation of existing weaknesses (e.g. basal crevasses) along which
76 the rift might be expected to preferentially propagate (Luckman et al., 2012). In Scenario I the
77 rift approaches the calving front by the shortest route via existing weaknesses, and so would
78 result in a reasonable minimum estimate for the calved area. In Scenario II the rift continues
79 along its current trajectory for a further 80km before approaching the ice front. The
80 hypothetical turning point in this scenario is chosen to smoothly continue the orientation of
81 the ice front where the rift will meet it (Fig. 1), and imitates the pattern of calving of a large
82 iceberg in 2008. We present these scenarios as reasonable possibilities for which to test the
83 impact of a calving event, rather than a range for the projected calved area. The eventual
84 calving may be within the range we test, or may be more extreme still.

85 **2.2 Numerical modelling**

86 To determine the influence of the potential calving event on the future stability of the
87 Larsen C Ice Shelf we use a numerical ice shelf model, previously applied to the Larsen B
88 (Sandhäger et al., 2005) and the Larsen C ice shelves (Jansen et al., 2010; Jansen et al., 2013;
89 Kulesa et al., 2014). This finite difference model is based on the continuum mechanical
90 equations of ice shelf flow. Friction at the ice shelf base as well as vertical shear strain due to
91 bending is neglected. Thus horizontal flow velocities are vertically invariant and the flow
92 field is two-dimensional. In the vertical dimension the model domain is divided into 13 levels,
93 scaled by ice thickness, to allow for a realistic vertical temperature profile, influencing the
94 vertically integrated flow parameter.

95 Simulations are carried out on a 2.5 km grid varying only the position of the ice shelf
96 calving margin between the present ice front position and rift Scenarios I and II. The model
97 we apply is a steady-state mode which assumes that the ice shelf is not in transition from one
98 geometry to another. It is important, therefore, to investigate the present stress field at the
99 predicted calving margin as well as the new stress field at the predicted calving margin under
100 the new geometries. These two states represent the stress field immediately after calving, and
101 the stress field towards which the shelf will develop in time through the process of the
102 velocity field adapting to the new geometry (assuming no immediate further calving). The
103 two stress fields may be different, and may indicate increasing or decreasing stability under
104 the new geometries.

105 **3 Results**

106 **3.1 Rift evolution and possible calving scenarios**

107 The rift first propagated into the Joerg Peninsula suture zone in 2012 and progressed during
108 2013 into a region which previously appeared to resist transverse fractures (Fig. 2). The rate
109 of rift propagation increased sometime between January and August 2014, crossing the entire
110 Trail Inlet flow unit (~ 20 km) in just 8 months. We do not have observations within this time
111 period so we cannot say whether the rift propagation during this time period was uniform or
112 was very rapid for only a short part of it. Between Aug. 2014 and late Jan. 2015, the rift
113 length increased further about 1.25 km, propagating into the next suture zone. From the start
114 of our measurements the width of the rift at the 2010 rift tip position has increased at a more
115 uniform rate than the length, and is still growing at a rate of ~40 m/year (Fig. 2).

116 The area of Larsen C Ice Shelf after the proposed calving event will be 4,600 km² less
117 than at present for Scenario I, and 6,400 km² less for Scenario II (Fig. 1). This amounts to
118 potential area losses of 9% and 12% respectively.

119 **3.2 Stress field development**

120 To investigate the impact of the two calving scenarios on ice shelf stability, we present
121 fields of the difference between the predicted directions of ice flow and of first principal stress
122 (the *stress-flow angle*; Fig. 3). This diagnostic has previously been used to investigate ice
123 shelf stability on the basis that existing weaknesses (rifts and crevasses) are typically oriented
124 across-flow (Kulesa et al., 2014). Regions of the shelf exhibiting low stress-flow angles are
125 likely to be more affected by small-scale calving because stresses act to open existing
126 weaknesses; conversely, regions with a stress-flow angle approaching 90° are likely to be
127 stable.

128 The stress-flow angles at the present (early 2015) ice front are generally high (Fig. 3a)
129 and, as a result, calving events are rare and the ice front is stable (Kulesa et al., 2014). If the
130 ice shelf calves under Scenario I, the new ice front will, in the immediate term, still mostly be
131 fringed by ice with a high stress-flow angle (Fig. 3a). However, this safety margin is
132 narrowed by the calving, and the centre of the new ice front will exhibit very low stress-flow
133 angles. Under this modest calving scenario, if the ice shelf is able to adapt to the new
134 geometry (Fig. 3b), a new region of high stress-flow angles develops, but this region remains
135 significantly narrower than at present. Under calving Scenario II, much more of the ice front
136 is immediately left without a buffer of high stress-flow angle ice (Fig. 3a). Even if it were
137 possible to adapt to this new geometry (Fig. 3c), a significant section of the new ice front
138 would retain very low values of stress-flow angle.

139 An alternative measure of stability was presented by Doake et al., (1998), whereby ice
140 downstream of a “compressive arch” represented by a contour of zero second principle stress
141 is subject to purely tensile stresses and regarded as a passive part of the ice shelf, its presence
142 indicating a stable front. This is a more conservative measure of stability than the stress-flow
143 angle and we include it for completeness. The dotted line in all panels of figure 3 represents
144 the zero second principal stress contour line for the reference simulation and the two new
145 calving fronts. For Scenario I this line is breached by the new calving front in the south at the
146 Gipps Ice Rise, for Scenario II it is breached on both sides.

147 4 Discussion

148 The rift highlighted here has been present since the earliest satellite imagery (Glasser et
149 al., 2009) but has recently propagated beyond its neighbouring structures to the point at which
150 a large calving event is anticipated. Over the past 4 years the rate of development of the rift
151 width has been steady, but the length has grown intermittently with a particular acceleration
152 during 2014 (Fig. 2). We hypothesize that the strain which opens the rift may be relatively
153 constant, but that the fracture response varies with tip position. This may be a result of
154 variations in fracture toughness of the ice which are likely to be related the presence of marine
155 ice in suture zones (Holland et al, 2009; Jansen et al., 2013) and the locations of pre-existing
156 weaknesses. The mean rate of rift propagation appears to be smaller when the rift tip is within
157 a suture zone (Fig. 2).

158 The reduction in area of Larsen C Ice Shelf under Scenarios I and II of 9% and 12%
159 respectively will be significant, but will of course not contribute to immediate sea level rise
160 since the floating ice already displaces its own weight of sea water. The predicted ice loss is
161 also not unprecedented: in the late 1980s a calving event removed 14% of Larsen C Ice Shelf
162 (Cook and Vaughan, 2010). The real significance of this new rift to this ice shelf is two-fold.
163 First, the predicted calving will reduce its area to a new minimum both in terms of direct
164 observations, and probably since the last interglacial period (Hodgson et al., 2006). Second,
165 unlike during the 1980s, but highly comparable to the development of Larsen B Ice Shelf
166 between 1995 and 2002, the resulting geometry may be unstable. According to the stress-flow
167 angle criterion, our calving scenarios lead to a range of unstable outcomes from partial to
168 significant. Under our modest rift propagation Scenario I, immediately following the
169 predicted calving event, the central part of the ice front will be unstable and prone to
170 persistent calving of small ice blocks as the principal strain works to open existing fractures.
171 It is not clear how quickly the velocity of a real ice shelf will be able to adapt to the new
172 boundary conditions, but even if this is rapid, the margin of stabilizing ice becomes very
173 narrow. Under Scenario II, the unstable part of the new ice front is considerably larger and,
174 even if the flow field adapts quickly to the new geometry, parts of the calving margin remain
175 unstable and prone to run-away calving of a similar nature to Larsen B Ice Shelf between
176 1995 and 2002. Assessing the stress field according to Doake et al. (1998), Scenario II would
177 also be considered as an unstable calving front.

178 Our model demonstrates that the newly developing rift presents a considerable risk to
179 the stability of the Larsen C Ice Shelf.

180 **5 Conclusions**

181 We have investigated a newly developing rift in the south of Larsen C Ice Shelf which
182 has propagated beyond its neighbours in 2013, and grew very rapidly in 2014. It seems
183 inevitable that this rift will lead to a major calving event which will remove between 9% and
184 12% of the ice shelf area and leave the ice front at its most retreated observed position. More
185 significantly, our model shows that the remaining ice may be unstable. The Larsen C Ice
186 Shelf may be following the example of its previous neighbour, Larsen B, which collapsed in
187 2002 following similar events.

188 **Acknowledgements**

189 The authors would like to thank Ted Scambos, Catherine Walker and Maurice Pelto for
190 their constructive comments which helped to improve this manuscript. This work was carried
191 out as part of the MIDAS project funded by NERC (NE/L005409/1) and continues work
192 carried out under the NERC SOLIS project (NE/E012914/1). D.J. was funded by the HGF
193 junior research group “The effect of deformation mechanism for ice sheet dynamics” (VHNG
194 802). We are indebted to NASA for the MODIS and Landsat data. D.J. would like to thank C.
195 Wesche for helpful discussions.

196 **References**

- 197 Borstadt, C. P., Rignot, E., Mouginot, J., and Schodlok, M. P., 2013. Creep deformation and buttressing capacity
198 of damaged ice shelves: Theory and application to Larsen C ice shelf. *The Cryosphere*, 7(6), 1931-1947.
- 199 Cook, A. J. and Vaughan, D. G., Feb. 2010. Overview of areal changes of the ice shelves on the Antarctic
200 Peninsula over the past 50 years. *The Cryosphere* 4 (1), 77-98.
- 201 Cook, A. J., T. I. Murray, A. Luckman, D. G. Vaughan, and N. E. Barrand. 2012. Antarctic Peninsula 100 m
202 Digital Elevation Model Derived from ASTER GDEM. Boulder, Colorado USA: National Snow and Ice
203 Data Center. <http://dx.doi.org/10.7265/N58K7711>.
- 204 Doake, C. S. M., Corr, H.F.J., Rott, H., Skvarca, P., and Young, N.W. 1998. Breakup and conditions for stability
205 of the northern Larsen Ice Shelf, Antarctica. *Nature*, 391 (6669), 778-780.
- 206 Glasser, N. F., Kulesa, B., Luckman, A., Jansen, D., King, E. C., Sammonds, P. R., Scambos, T. A., and Jezek,
207 K. C., 2009. Surface structure and stability of the Larsen C Ice Shelf, Antarctic Peninsula. *Journal of*
208 *Glaciology* 55 (191), 400–410. URL <http://dx.doi.org/10.3189/002214309788816597>

209 Hodgson, D. A., Bentley, M. J., Roberts, S. J., Smith, J. A., Sugden, D. E., and Domack, E. W., Aug. 2006.
 210 Examining Holocene stability of Antarctic Peninsula ice shelves. *Eos Trans. AGU* 87 (31), 305-308. URL
 211 <http://dx.doi.org/10.1029/2006eo310001>

212 Holland, P. R., Corr, H. F. J., Vaughan, D. G., Jenkins, A., and Skvarca, P., 2009. Marine ice in Larsen Ice Shelf.
 213 *Geophysical Research Letters* 36 (11), L11604+. URL <http://dx.doi.org/10.1029/2009GL038162>

214 Holland, P. R., Corr, H. F. J., Pritchard, H. D., Vaughan, D. G., Arthern, R. J., Jenkins, A., Tedesco, and M.,
 215 May 2011. The air content of Larsen Ice Shelf. *Geophysical Research Letters* 38 (10), L10503+. URL
 216 <http://dx.doi.org/10.1029/2011GL047245>

217 Holland, P. R., Brisbourne, A., Corr, H. F. J., McGrath, D., Purdon, K., Paden, J., Fricker, H. A., Paolo, F. S.,
 218 and Fleming, A. H., Jan. 2015. Atmospheric and oceanic forcing of Larsen C Ice Shelf thinning. *The*
 219 *Cryosphere Discussions* 9 (1), 251-299.

220 Jansen, D., Kulesa, B., Sammonds, P.R., Luckman, A., King, E. C., and Glasser, N. F, 2010, Present stability of
 221 the Larsen C Ice Shelf, Antarctic Peninsula, *Journal of Glaciology*, Volume: 56, Issue: 198, Pages: 593-600

222 Jansen, D., Luckman, A. J., Kulesa, B., Holland, P. R. and King, E. C., 2013. Marine ice formation in a suture
 223 zone on the Larsen C Ice Shelf and its influence on ice shelf dynamics. *Journal of Geophysical Research:*
 224 *Earth Surface*, 118, 1-13, doi: 10.1002/jgrf.20120

225 Khazendar, A., Rignot, E., and Larour, E., 2009. Roles of marine ice, rheology and fracture in the flow and
 226 stability of the Brunt/Stancomb-Wills Ice Shelf, *Journal of Geophysical Research*, 114, F04007, doi:
 227 10.1029/2008JF001124.

228 Khazendar, A., Rignot, E., and Larour, E., 2011. Acceleration and spatial rheology of Larsen C Ice Shelf,
 229 Antarctic Peninsula, *Geophysical Research Letters*, 38, L09502, doi: 10.1029/2011GL046775.

230 Kulesa, B., Jansen, D., Luckman, A. J., King, E. C., and Sammonds, P. R., 2014. Marine ice regulates the future
 231 stability of a large Antarctic ice shelf. *Nature communications*, doi: 10.1038/ncomms4707

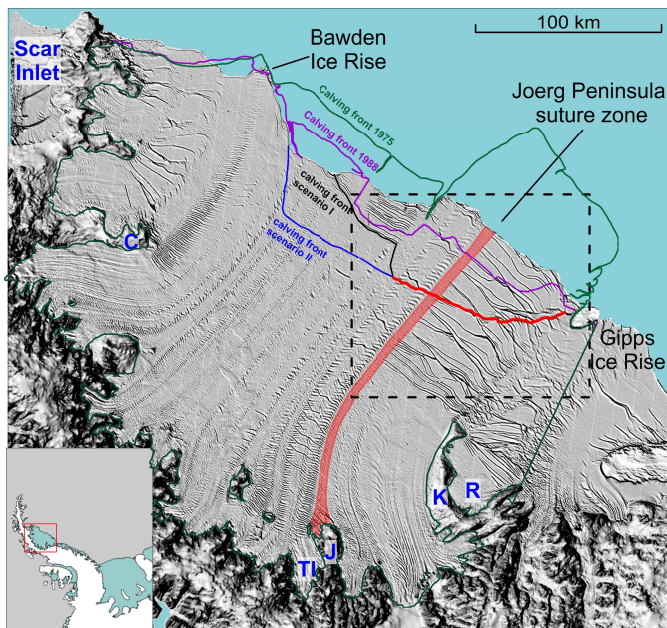
232 Luckman, A. J., Jansen, D., Kulesa, B., King, E. C., Sammonds, P.R., and Benn, D. I., 2012. Basal crevasses in
 233 Larsen C Ice Shelf and implication for their global abundance. *The Cryosphere*, 6, 113-123, doi: 10.5194/tc-6-
 234 113-2012.

235 Luckman, A. J., Elvidge, A., Jansen, D., Kulesa, B., Kuipers-Munneke, P., and King, J., 2014. Surface melt and
 236 ponding on Larsen C Ice Shelf and the impact of föhn winds. *Antarctic Science*, 26(6), 625-635, doi:
 237 10.1017/S0954102014000339.

238 McGrath, D., Steffen, K., Holland, P.R., Scambos, T. S., Rajaram, H., Abdalati, W., Rignot, E., 2014. The
 239 structure and effect of suture zones in the Larsen C Ice Shelf, Antarctica. *Journal of Geophysical Research:*
 240 *Earth Surface*, 119, 588-602, doi: 10.1002/2013JF002935.

241 Pritchard, H. D., Ligtenberg, S. R. M., Fricker, H. A., Vaughan, D. G., van den Broeke, M. R., and Padman, L.,
 242 Apr. 2012. Antarctic ice-sheet loss driven by basal melting of ice shelves. *Nature* 484 (7395), 502-505.

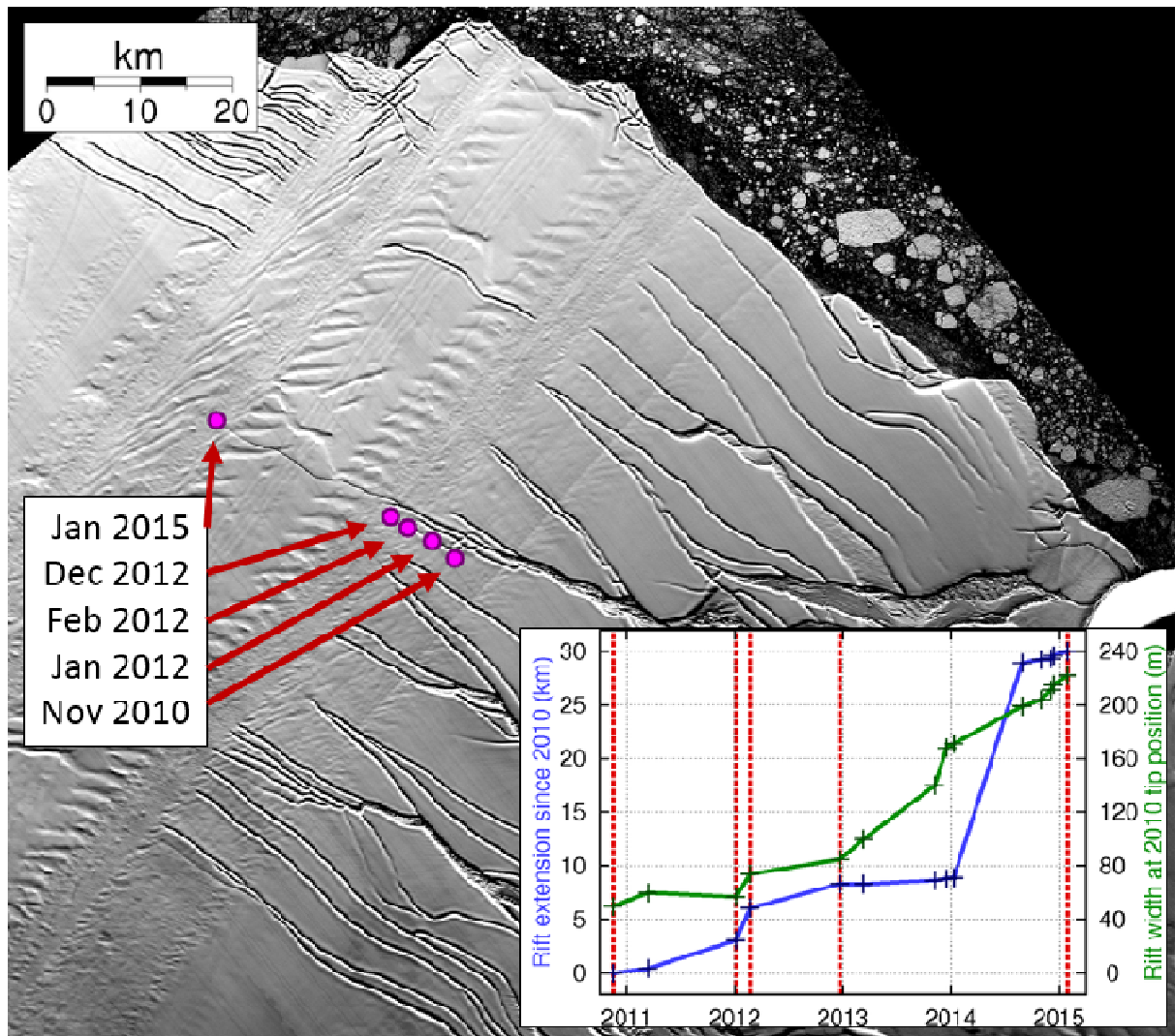
- 243 Sandhäger, H., Rack, W., and Jansen, D., 2005. Model investigations of Larsen B Ice Shelf dynamics prior to the
244 breakup. Forum for Research into Ice Shelf Processes (FRISP), Report, 16, 5-12, Bjerknes Cent. For Clim.
245 Res., Bergen, Norway.
- 246 Shepherd, A., Wingham, D., Payne, T., and Skvarca, P., Oct. 2003. Larsen Ice Shelf has progressively thinned.
247 Science 302 (5646), 856-859.
- 248 Vanden Broeke, M., Jun. 2005. Strong surface melting preceded collapse of Antarctic Peninsula ice shelf.
249 Geophys. Res. Lett. 32 (12), L12815+.
- 250



251

252 **Figure 1:** Overview of the Larsen C Ice Shelf in late 2014 showing the contemporary location
 253 of the developing rift (red line), and a selection of previous and predicted future calving
 254 fronts. Background image is MODIS Aqua, Dec. 3rd 2014 for the ice shelf and a shaded relief
 255 DEM of the Antarctic Peninsula mountains: Cook et al. (2012). Geographic features of
 256 interest are marked (TI = Trail Inlet, K = Kenyon Peninsula, R = Revelle Inlet, J = Joerg
 257 Peninsula, C= Churchill Peninsula) and the dashed box shows the extent of Figure 2. The
 258 highlighted flow line indicates the location of the Joerg Peninsula suture zone.

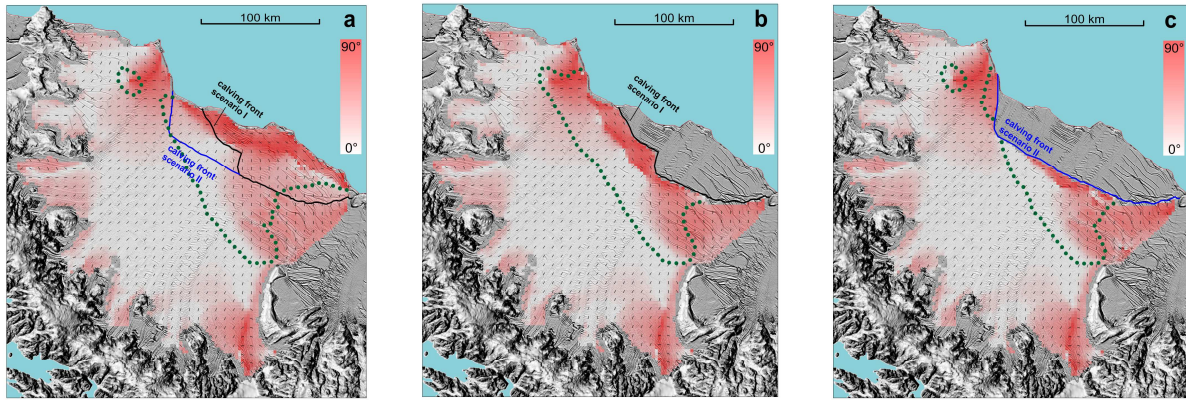
259



260

261 **Figure 2:** Analysis of rift propagation using Landsat data. Background image, in which the
 262 rift is visible, is from Dec 4th 2014. Inset graph shows the development of rift length with
 263 respect to the 2010 tip position, and rift width at the 2010 tip position, measured from all
 264 available Landsat images (crosses; 15 in total). The line joining data points illustrates only the
 265 mean propagation rate between observations. Actual propagation of the rift may be sporadic
 266 and true propagation rates cannot be known without regular frequent observations which are
 267 not available. Circles and labels on the map, and dotted red lines on the graph, show the
 268 positions of notable stages of rift development.

269



270

271 **Figure 3:** Results from ice shelf flow model: Stress-flow angle fields for the present day ice
 272 front geometry (a) and for the new geometries under Scenarios I (b) and II (c). The green
 273 dotted line represents the contour line of zero second principal stress.

274